# Computationally Guided Tuning of Amino Acid Configuration Influences the Chiroptical Properties of Supramolecular Peptide-π-Peptide Nanostructures

Sayak Subhra Panda,[†,‡] Kirill Shmilovich[¶], Andrew L. Ferguson[¶], and John D. Tovar[*,†,‡,⊥]

[†] Department of Chemistry, Johns Hopkins University, 3400 North Charles Street, Baltimore, Maryland 21218, United States.

[‡] Institute of NanoBioTechnology, Johns Hopkins University, 3400 North Charles Street, Baltimore, Maryland, 21218, United States.

[⊥] Department of Materials Science and Engineering, Johns Hopkins University, 3400 North Charles Street, Baltimore, Maryland 21218, United States.

[¶] Pritzker School of Molecular Engineering, University of Chicago, 5640 South Ellis Avenue, Chicago, Illinois, 60637, United States.

[*]Corresponding author email: tovar@jhu.edu

## Abstract:

Self-assembled supramolecular materials derived from peptidic macromolecules with π-conjugated building blocks are of enormous interest because of their aqueous solubility and biocompatibility. The design rules to achieve tailored optoelectronic properties from these types of materials can be guided by computation and virtual screening rather than intuition-based experimental trial-and-error. Using machine learning, we reported previously that supramolecular chirality in self-assembled aggregates from VEVAG-π-GAVEV type peptidic materials was most strongly influenced by hydrogen bonding and hydrophobic packing of the alanine and valine residues. Herein, we build upon this idea to demonstrate through molecular-level experimental characterization and all-atom molecular modeling that varying the stereogenic centers of these residues has a profound impact on the optoelectronic properties of the supramolecular aggregates, whereas the variation of stereogenic centers of other residues has only nominal influence on these properties. This study highlights the synergy between computational and experimental insight relevant to the control of chiroptical or other electronic properties associated with supramolecular materials.

## Introduction:

Chirality at both the molecular and supramolecular levels plays a pivotal role in chemistry, biology, physics and material sciences, impacting applications such as biosensors, pharmaceutics, chiral catalysis, asymmetric synthesis, and non-linear optics.[1-10] In this respect, the spontaneous aggregation of chiral or achiral small molecular counterparts to form hierarchical chiral nanostructures influenced by non-covalent interactions such as hydrogen-bonding, π-stacking, van der Waals interactions and steric effects have been well explored.[11-15] In addition to molecular influences, external effects such as solvent,[16-18] temperature,[19-21] pH,[22, 23] photo-irradiation[24], sonication[25] and additives[26, 27] can exert a profound effect on supramolecular chirality and the morphology of the resulting nanostructures. For example, in a perylene appended sugar molecule, the handedness of the helical structure that formed depends on the solvent polarity.[18] Temperature-induced supramolecular chirality and morphology changes were observed for nanostructures comprised of 1,3,5-benzenetriscarboxylic esters and amides.[21] These studies exemplify the complexity associated with assigning the chiral nature of supramolecular nanostructures from their molecular character.

Oligopeptides are appealing molecular building blocks due to their ease of solid-phase synthesis, tunable hydrophobicity and diversity available through amino acid structure, all of which lead to the formation of diverse superstructures. Varying the stereogenicity of the constituent amino acids is an effective strategy to control the evolution of supramolecular chirality.[28-34] In general, these molecular level "point mutations" are regarded as key factors in determining the chirality of hierarchical peptide and protein structures due to the changes in folding propensities and subsequent supramolecular organization. Naturally occurring L-amino acids usually form right-handed β-strands upon folding, which give rise to left-handed twists in β-

sheets formed by hydrogen-bonding between β-strands. Contrariwise, D-amino acids normally form right-handed twists in the β-sheets upon aggregation. For example, Wang *et al*. reported a switch in handedness of supramolecular nanostructures with the change in configuration of the lysine head group.[28] Profound effects of switching the configuration of constituent amino acids in superstructures formed from tripeptides were also explored by CD spectroscopy.[29] Beyond stereogenic D/L variation, peptidic superstructures are also affected by other variables such as sequence and composition of the constituent amino acids. Cui *et al*. designed four different peptide amphiphiles by varying valine and aspartic acid adjacent to a hydrophobic alkyl group, which showed that alternating hydrophobic and hydrophilic groups has a profound effect on the hierarchical structure.[30] Xing *et al*. showed how the hydrophobicity change along the polypeptide backbone changes the handedness of the hierarchical structure.[31] Several hypotheses were proposed to justify the different handedness of the short polypeptides and proteins based on their terminal group interaction, altering hydrophobicity and incubation conditions, but design principles correlating the supramolecular chirality and handedness of the supramolecular nanostructures with the structure of the molecular counterparts are largely lacking for peptidic materials.

The formation of hierarchical structure from π-chromophores appended with peptides is of significant interest due to their prospect for electronic applications in aqueous media,[35-43] where the local supramolecular chirality would be expected to impact the through-space interactions of the chromophores' transition dipoles, leading to variations in exciton coupling. These same intermolecular interactions could be exploited for optoelectronic applications such as field-effect transistors and organic solar cells.[44-54] Amino acids present in peptide-π hybrid materials are also known to impact the chirality of the hierarchical structure formed.[55-62] For example, Pandeeswar

*et al*. observed that the configuration of the first amino acid plays an important factor in controlling the supramolecular chirality in a dipeptide appended to a naphthalene diimide core.[55] Schillinger *et al*. controlled the chirality of the superstructure formed from an oligothiophene core by the stereochemistry of an appended proline residue.[57] Marty *et al*. identified a two-fold odd even effect as manifested in circular dichroism (CD) spectroscopy when the number of L-alanine units and spacer lengths were varied in a perylene diimide system appended with oligopeptide/polymer conjugates.[56] These studies exemplify the complexity associated with the emergent helicities of the superstructures formed from molecular counterparts and hence a detailed and comprehensive study is needed to understand the superstructure formation from these peptide-π systems.

We recently discovered a way to control chirality of supramolecular nanostructures through incorporation of saturated, non-conjugated alkyl spacer groups between peptidic and π-chromophoric regions of self-assembling molecules.[63] We identified that an even number of alkyl carbons (0, 2) in the spacer units induce M-type supramolecular aggregates, similar to left-handed twists, whereas an odd number of alkyl carbons (1, 3) in the spacer units induce P-type helical character, similar to right-handed twists (**Figure 1**). Using "white box" machine learning approaches designed to admit transparent physical interpretability, we also identified the key atoms/residues responsible for determining chiral packing of the supramolecular motif (**Figure 1**). While many of the highly ranked atoms were part of the oligopeptide amide bonds involved in promoting intermolecular hydrogen bonding within the self-assembled structures, a few of the off-backbone carbon atoms on the side chains also ranked highly. Herein, we challenge and corroborate this finding by showing how the variation of molecular level configuration associated with these off-backbone atoms/residues (through the use of D/L amino acids) allow for further manipulation of the supramolecular chirality with unprecedented levels of diversity, whereas

variation in other atoms/residues which were not indicated to be important does not have significant impact. We found that variation of configuration of the constituent amino acids can change the handedness of the self-assembled chiral nanostructures in addition to additive chirality tuning by alkyl spacer length variation. This synergistic level of control will offer predictive electronic property design towards the continued development of peptide-π conjugated materials in chiroptical phenomena that would require chiral materials capable of selective interaction with circularly polarized light.

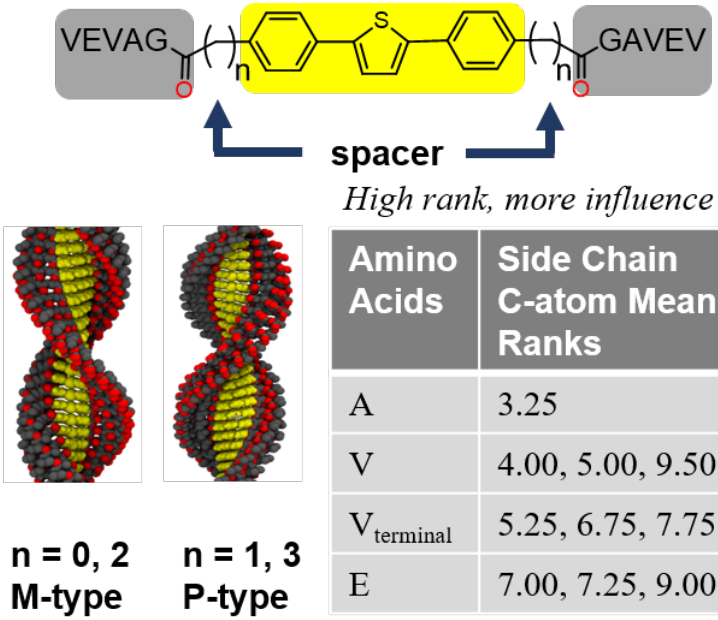


| Amino Acids | Side Chain C-atom Mean Ranks |
|---|---|
| A | 3.25 |
| V | 4.00, 5.00, 9.50 |
| $V_{terminal}$ | 5.25, 6.75, 7.75 |
| E | 7.00, 7.25, 9.00 |

**Figure 1**. Peptide-π-peptide molecules (top) formed chiral nanostructures that varied with alkyl spacer length (bottom left). They were subjected to interpretable machine learning methods that ranked several residue-centered carbon atoms as having a key influence on the observed chiralities (bottom right).

## Experimental Section:

**General Information.** *N*,*N*-dimethylformamide (DMF) was purchased from Sigma-Aldrich. *N*-methyl-2-pyrrolidone (NMP) was obtained from Advanced ChemTech. Dichloromethane (DCM) and n-hexane were freshly distilled prior to storage. All solvents were stored over 4 Å molecular

sieves and were subsequently degassed by sparging with nitrogen gas at least 30 min prior to use. *O*-(Benzotriazol-1-yl)-*N,N,N′,N′*-tetramethyluronium hexafluorophosphate (HBTU), 3-(4-bromophenyl)propionic acid, 4-bromophenylacetic acid, and 4-(4-bromophenyl)butanoic acid were purchased from Oakwood Products Inc. Tetrakis(triphenylphosphine)palladium was obtained from Strem Chemicals. Wang resin (pre-loaded with amino acid) and Fmoc-protected amino acids were obtained from Advanced Chem Tech. 4-iodobenzoic acid was purchased from Alfa Aesar. Biotech grade cellulose ester dialysis tubing (MWCO 500-1000) was purchased from Spectrum Labs. All other reagents and starting materials were obtained from Sigma-Aldrich and were used as received.

*NMR Spectroscopy.* $^{1}$H-NMR spectra were obtained using a Bruker Advance 400 MHz FT-NMR spectrometer and processed with Bruker Topspin 1.3. Peptide $^{1}$H NMR spectra were acquired using a presaturation pulse to suppress water. Chemical shifts are reported in parts per million relative to the residual protio solvent [HOD δ: 4.79, $CHCl_3$ δ: 7.26].

*Electrospray Ionization Mass Spectrometry (ESI-MS).* ESI samples were collected using a Thermo Finnigan LCQ Deca Ion Trap Mass Spectrometer in negative mode. Samples were prepared in a 1:1 MeOH:water solution with 1% ammonium hydroxide.

*Reverse-Phase HPLC*. HPLC purification was performed on an Agilent 1100 series (semi-preparative/analytical) and a Varian PrepStar SD-1 (preparative) instruments using Luna 5 μm particle diameter C8 with TMS endcapping columns with silica solid support. An ammonium formate aqueous buffer (pH 8) and acetonitrile was used as the mobile phase.

*UV-Vis and Photoluminescence*. UV-Vis spectra were obtained using a Varian Cary 50 Bio UV-Vis spectrophotometer. Photoluminescence spectra were obtained using a PTi Photon Technology

International Fluorometer (QuantaMaster 40) with a 75-W Ushio Xenon short arc lamp and operated with Felix32 Version 1.2 software. Spectroscopic samples were prepared by diluting the peptide solution to the appropriate concentration (exact concentrations given in spectra captions) in Millipore water to achieve an optical density near 0.1. The pH was then adjusted by adding 30 μL of 2M KOH (basic) followed by addition of 80 μL of 2M HCl (acidic).

*Circular Dichroism (CD).* CD spectra were obtained using a Jasco J-810 spectropolarimeter. Spectroscopic samples were prepared by diluting the peptide solution to the appropriate concentration (exact concentrations given in spectra captions) in Millipore water. The pH was then adjusted by adding 30 μL of 2M KOH (basic) followed by addition of 80 μL of 2M HCl (acidic).

*Dynamic Light Scattering (DLS).* DLS spectra were obtained using a Zetasizer Nano-ZS90 (Malvern Instruments). Spectroscopic samples were prepared by diluting the peptide solution to the appropriate concentration (exact concentrations given in spectra captions) in Millipore water. The pH was then adjusted by adding 30 μL of 2M KOH (basic) followed by addition of 80 μL of 2M HCl (acidic).

*Attenuated total reflection Fourier transform infrared (ATR-FTIR)*. ATR-FTIR spectra were obtained on lyophilized acidic peptide solutions using a Thermo Scientific Nicolet iD5 ATR-IR.

*Transmission Electron Microscopy (TEM)*. Imaging was performed on a Philips EM 420 transmission electron microscope equipped with an SIS Megaview III CCD digital camera at an accelerating voltage of 100 kV. Acidic solutions (0.25-0.35 wt%) of each peptide were prepared by placing the samples in a closed container with a vial of conc. HCl opened within, which initiated the assembly process by diffusion of HCl vapor to the sample. The assembled peptides in water were pipetted (drop of 1 mg/mL solution) onto 200 mesh copper grids coated with carbon and

incubated for 5 minutes at 25°C. Excess solution was wicked off by touching the side of the grid to filter paper. The samples were then stained with a 2% uranyl acetate solution and excess moisture was wicked off. The grid was allowed to dry in air before imaging.

**General Solid Phase Peptide Synthesis (SPPS)**. All peptides were synthesized using the standard Fmoc solid phase technique with Wang resin pre-loaded with Fmoc-protected valine (Wang-Val, 0.700 mmol/g). To the resin in a peptide chamber, Fmoc-deprotection was accomplished by adding a 20% piperidine solution in DMF twice (successive 5-and 10-minute treatments) followed by washing with NMPx3, methanolx3 and DCMx3. For the amino acid couplings, 3.0 equiv of the Fmoc-protected amino acid was activated with 2.9 equiv of HBTU and 10 equiv diisopropylethylamine (DIPEA) in NMP, and this solution was added to the resin beads. The reaction mixture was allowed to mix for 45–90 minutes, after which the beads were rinsed with NMP, methanol and DCM (3 times each). The completion of all couplings was monitored using a Kaiser test on a few dry resin beads, repeating the same amino acid coupling as needed. The general procedure for amino acid coupling was repeated for each additional amino acid until the desired peptide sequence was obtained.

**General N-acylation Procedure for Peptides**. Following our previous procedure, a solution containing 3 equiv of aryl halide carboxylic acid, HBTU (2.9 equiv) and DIPEA (10 equiv) in NMP was mixed with the oligopeptide-bound resin for 3 h. The completion of the N-acylation was assessed using a Kaiser test on a few dry resin beads. The resin was washed with NMP, methanol and DCM (3 times each).

**General on-Resin Stille Coupling Procedure.** The solid supported oligopeptide capped with an aryl halide (1 equiv) was transferred to a Schlenk flask equipped with a reflux condenser. The resin was dried under vacuum. $Pd(PPh_3)_4$ (4 mol%, relative to resin loading) was added to the reaction

vessel. An approximately 15 mM solution of the 2,5-bis(trimethylstannyl)thiophene (0.50 eq) was prepared in DMF and was added to the reaction flask via syringe. The mixture was heated to 80°C for 16-21 h and was agitated constantly by bubbling nitrogen through the solution. The mixture was allowed to cool to room temperature. The peptide was subjected to the general cleavage and work-up procedure to yield the crude product, then further purified by HPLC.

**General Peptide Cleavage and Work-up Procedure.** Following solid-phase cross-coupling, the resin was returned to the peptide chamber and again subjected to a standard wash cycle: 3x NMP, 3x DMF, 3x methanol and 3x DCM. The resin was treated with 9.50 mL of trifluoroacetic acid, 250 μL water, and 250 μL of triisopropylsilane for 3 h. The peptide solution was filtered from the resin beads, washed 3x with DCM, and was concentrated by evaporation under reduced pressure. The crude peptide was then precipitated from solution with 60-80 mL of diethyl ether and isolated through centrifugation. The resulting pellet was triturated with diethyl ether to yield crude product, which was dissolved in approximately 10-15 mL of water and 50 μL potassium hydroxide (1M) and lyophilized. The solution was placed inside dialysis tubing of the appropriate length. The tubing was stirred in 1L of water for 1 h, the water was exchanged, and the tubing was allowed to stir for another 1 h. This process was repeated twice and then the tubing stirred overnight (approx. 15 h). The tubing was removed from water, and the peptide solution transferred to a separate container and lyophilized.

**Molecular Simulations.** Simulations were performed using the Gromacs 2019.2 simulation suite[64] and linked with PLUMED version 2.5 libraries[65] employing a similar protocol to that which we previously reported.[63] Initial all-atom configurations and topologies of each π-conjugated peptide was generated using the Automated Topology Builder (ATB) server[66] and modeled with the GROMOS 54a7 force field[67]. Each metadynamics simulation considers two π-conjugated peptides

which were prepared as a dimer by initializing initial configurations with a center of mass separation of 0.45 nm and a relative twist angle of $\theta$ = +10° (see **Eqn. 1**). These initial conditions for $|d|$ and $\theta$ were selected to avoid high energy overlaps in the initial conformation of two molecules while remaining within our definition of a dimer where $|d| < 0.6$ nm. The dimer was solvated in water modeled using a simple point charge (SPC) model[68] within a simulation box with 1.5 nm spacing between the solute and box edges, amounting to an approximately 7 x 6 x 5 $nm^3$ simulation box, to mimic an isolated dimer at infinite dilution. Periodic boundary conditions were applied in all three dimensions. The system was prepared in a protonation state corresponding to pH 1 consistent with the low-pH conditions under which experimental assembly is observed. All amino acids are charge neutral under these conditions, and so it was not necessary to add any counter-ions to neutralize excess system charge. The initial system configurations were then equilibrated using steepest descent energy minimization removing forces larger than 10 kJ/mol.nm followed by a 100 ps NVT equilibration run at 300 K and a 100 ps NPT equilibration run at 300 K and 1 bar during which the temperature, pressure, and density were observed to stabilize. Initial velocities were generated sampling from a Maxwell-Boltzmann distribution at 300 K. Lennard-Jones interactions were shifted smoothly to zero at 1.0 nm. The leap-frog algorithm with a 2 fs time step was used to numerically integrate Newton's equations of motion[69]. All covalent hydrogen bonds were held fixed with the LINCS algorithm[70]. Coulomb interactions were treated by Particle Mesh Ewald (PME) with a real space cutoff of 1.0 nm and a 0.16 nm Fourier grid spacing, with both of these values tuned during runtime for optimized performance[71]. Temperature was controlled by a velocity-rescaling thermostat[73] and pressure by a Parrinello-Rahman barostat[74].

Production runs implementing well-tempered metadynamics[72] were subsequently performed in the NPT ensemble where the temperature was maintained at 300 K using a velocity-

rescaling thermostat[73] and pressure at 1 bar employing a Parrinello-Rahman barostat[74]. Trajectory snapshots were saved every 10 ps for analysis. Metadynamics enhanced sampling was performed along a single collective variable (CV) defined as the signed twist angle $\theta$ between dimer pairs of π-conjugated peptides (see Eqn. 1). Gaussians were deposited with a pace of 1 ps, width of 0.2 radians, initial height of 1.2 kJ/mol.rad, and a bias factor of $\gamma = 5.0$. Harmonic restraining potentials with force constants of 500 kJ/mol.nm and 500 kJ/mol.rad were applied if the center of mass separation between the π-conjugated cores exceeded $|\boldsymbol{d}| > 0.6$ nm and if twist angle exited the window $\theta$ = [-1.25,1.25] radians, respectively, in order to maintain integrity of the dimer pair. Each production run was initially performed for 2 μs and extended in intervals of 500 ns until the metadynamics simulation converged. Convergence was typically achieved in 2-7 μs of simulation and defined by the dual criteria that (i) the height of the deposited Gaussians plateaued to near zero and (ii) approximately uniform sampling in the CV $\theta$ was observed (i.e., an approximately flat histogram) defined by the fraction of configurations with $\theta > 0$ and $\theta < 0$ were within ~5%. Five independent metadynamics simulations were run to convergence for each π-conjugated peptide. Each simulation employs the same initial structure and metadynamics parameters, but are initialized with different random velocities, which, by the chaotic nature of molecular simulations, assure the simulations rapidly decorrelate and become independent[75]. Estimates of the unbiased probability distribution in the signed twist angle $P(\theta)$ over the range $\theta$ = [-1.25,1.25] radians were recovered by employing reweighting to eliminate the bias imposed by the metadynamics potential.[76]

## Results:

The pH-driven assembly of peptide-π-electron-peptide molecules has been extensively studied, where deprotonated carboxylic acids promote molecular dissolution at basic pH (ca. pH 11) while

protonation and charge screening under acidic conditions (ca. pH 2) foster self-assembly.[63, 77] In line with previous work, these assemblies also enforce 'H-type' aggregates where the transition dipoles of interacting molecules are oriented in a cofacial fashion. This assembly results in a hypsochromic shift in absorption maxima along with bathochromic shift and quenching of emission maxima.[78] After the assembly, an induced circular dichroism (CD) signal is observed around the absorption maximum, indicating exciton coupling of the interacting chromophores as held within a chiral environment. Transmission Electron Microscopy (TEM) of these materials indicates the formation of 1D aggregates with widths on the order of 10 nm. In this work, we describe how the stereogenic centers of the constituent amino acids impact the local chiral environments of the interacting chromophores upon self-assembly.

**Design:** We targeted a series of peptide-π-peptide molecules that varied the stereogenic centers (D/L residues) of two of the component amino acids in the VEVAG sequence – the internal valine and the alanine residues – which molecular modeling and machine learning previously identified as key molecular points for affecting the supramolecular chirality and packing of diphenyl thiophene (PTP) π-conjugates.[63] We simultaneously varied alkyl spacer length (between 0-3 carbons) in between the peptidic and π-conjugated regions to further explore the chirality tuning according to our previous work.[63] We also altered the stereogenic center of the valine residues at the peptide termini to understand how supramolecular chirality is affected by a change in a residue that was not identified as a key component to determine supramolecular chirality. This library was prepared according to our prior reports using on-resin Pd-catalyzed dimerization to flank the central diphenyl thiophene core with the VEVAG sequences, only using the respective D or L amino acid as needed during Fmoc-based solid phase peptide synthesis.

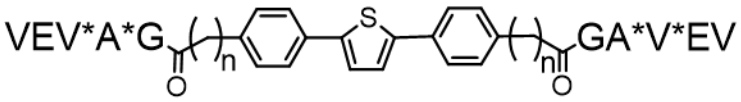


| n = 0 | n = 1 | n = 2 | n = 3 |
|---|---|---|---|
| $V_LA_L$-0 | $V_LA_L$-1 | $V_LA_L$-2 | $V_LA_L$-3 |
| $V_LA_D$-0 | $V_LA_D$-1 | $V_LA_D$-2 | $V_LA_D$-3 |
| $V_DA_L$-0 | $V_DA_L$-1 | $V_DA_L$-2 | $V_DA_L$-3 |
| $V_DA_D$-0 | $V_DA_D$-1 | $V_DA_D$-2 | $V_DA_D$-3 |

**Figure 2**. Peptides synthesized with varying amino acid configuration and spacer of different π-chromophore. $V_DEV_LA_LG$-0 was also synthesized.

**Photophysics:** The photophysical properties of different families of peptide-spacer-π block molecules upon assembly give insight about how the local amino acid chirality impacts hierarchical structures, even though the responses should be treated as ensemble averages of various local chromophore interactions within a particular nanostructure. Following the trends associated with 'H-type' co-facial chromophore interactions, absorption maxima of each peptide shifted to lower wavelength upon self-assembly under acidic pH as compared to the molecularly dissolved sample at basic pH. However, the magnitude of the blue shift varied significantly with the stereochemistry of the component amino acid, irrespective of the spacer length incorporated within. Assemblies where valine and alanine were both in the L configuration ($V_LA_L$) and were both in the D configuration ($V_DA_D$) imparted the most substantial blue shifts (30 nm for 0-spacer and 23 nm for 1- , 2- and 3-spacer). Sequences where valine and alanine had different stereogenic configurations (e.g. $V_DA_L$ and $V_LA_D$) showed much more subtle blue shifts in their respective assemblies (3-7 nm for 0-spacer, 10 nm for 1- and ~15 nm for 2- and 3-spacer). (Representative spectra can be found for the VxAx-0 family are shown in **Figure 3a,** and spectra for the other families are in **Figure S53-S55**). We note that the differences in the observed shifts from basic to

acidic solution between ($V_LA_L$,$V_DA_D$) and ($V_LA_D$,$V_DA_L$) become smaller with increasing spacer length: ~25 nm for 0-spacer, 13 nm for 1-spacer, 8 nm for 2- and 3-spacer (**Table S2**).

In line with previous work, monomeric peptides with embedded alkyl spacer units show more structured emission signals with clear vibronic signatures whereas no spacer peptides showed unstructured features.[63] Within each family (0-, 1-, 2- and 3-spacer) distinct signatures were recorded for peptides with varying configuration of individual amino acids. Photoluminescence spectroscopy corroborated the idea that $V_LA_L$-0 and $V_DA_D$-0 form nanostructures where the embedded chromophores interact more intimately as compared to other molecules which is evident from the stronger quenching that is indicative of stronger H-type cofacial exciton coupling. It appears that $V_DA_L$-0 and $V_LA_D$-0 do not form as tightly coupled nanostructures based on their smaller PL red shifts and less quenching (**Figure 3b**). For the 1-spacer family, $V_DA_L$-1 also yielded the lowest red-shift, and structured features were present in the assembled form. The assembled $V_LA_D$-1 also maintained the vibronic emission profile although with higher quenching in the signal. $V_LA_L$-1 and $V_DA_D$-1 showed highest quenching and red-shift similar to the 0-spacer family (**Figure S56**). Other peptide families (2- and 3-spacer) followed the similar pattern as of 1-spacer molecules both in monomeric and assembled form except for $V_DA_D$-3/$V_LA_L$-3 (**Figure S57, S58**). These results suggest that the configuration of individual amino acids significantly affects the electronic couplings within the assembled supramolecular nanostructures.

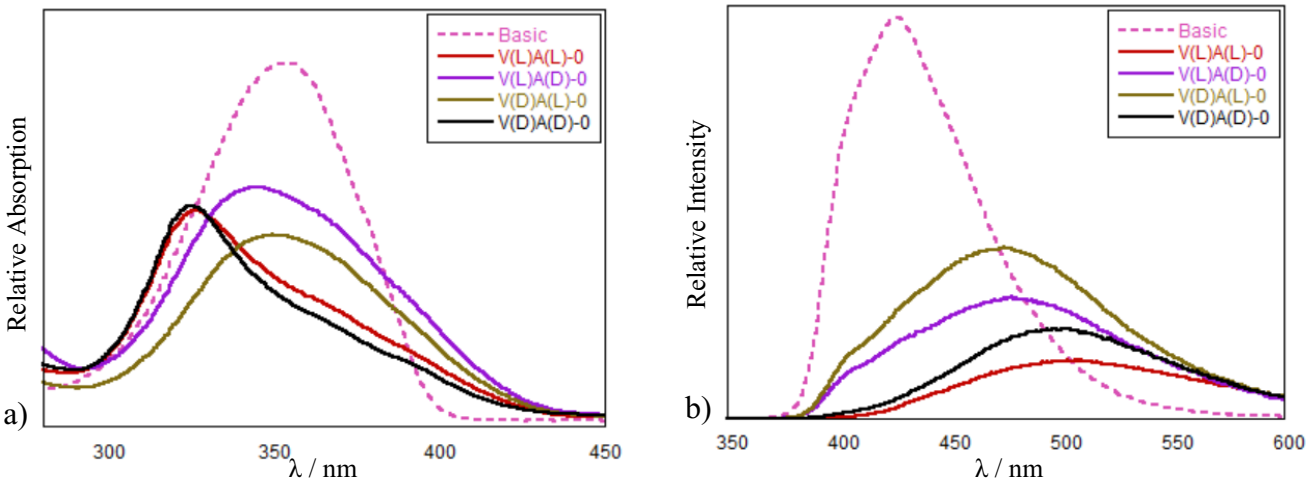


**Figure 3**. UV−vis (a) and PL (b) spectroscopy of 0-spacer under acidic conditions acquired at a concentration of 30 μM. Basic solutions were made by adding 30 μL of KOH (2 M) and acidified by adding 50 μL of HCl (2 M) to the basic solution. Normalized basic solutions are represented by dashed line.

Chiroptical properties were revealed through CD spectroscopy. CD is typically used to characterize peptide n-π* transition dipoles which can inform on different secondary structures;[79] however, the molecules studied here only showed red-shifted β-sheet type signatures in the amide bond region. $V_LA_L$ and $V_DA_D$ present opposite high-energy CD signatures that were consistent in all different alkyl spacer series regardless of spacer length. $V_LA_D$ peptides showed a similar pattern across all the peptides irrespective of spacer length whereas $V_DA_L$ 0-spacer peptides showed a different signature from 1-,2- and 3-spacer peptides. (**Figure S60**). FT-IR spectra from lyophilized solid peptides demonstrated amide I signatures at ca. 1625-1640 $cm^{-1}$ which correlated with β-sheet-type signature (**Figure S49-S52**).

More importantly for this study, bisignate Cotton effects indicated the exciton coupling of the π-π* electronic transition dipoles associated with the PTP chromophores.[80] The molecularly dissolved samples did not show any spectral responses in the π-π* region, but after assembly, visible bisignate Cotton effects were observed where the crossover point coincided with the

chromophore's absorption maxima. In our earlier work, we observed an odd-even effect in the bisignate signal handedness and intensity for all the $V_LA_L$ peptides depending on the spacer length between the PTP π-core and the peptidic region: peptides with 0- and 2-carbon spacers yielded M-type helical supramolecular aggregates (based on the negative split signal at higher wavelength and positive signal at lower wavelength region), which correlate to left-handed supramolecular twists in natural β-sheet type peptides, whereas 1- and 3-carbon spacer peptides formed P-type helical supramolecular aggregates (positive signal at higher wavelength and negative signal at lower wavelength), which correlate to right-handed supramolecular twists. In this work, we observed that all $V_DA_D$ peptides formed P-type supramolecular aggregates irrespective of the spacer length (**Figure 4, Table S3**). Odd-even effects were pronounced in the intensity of the Cotton effect where 0-spacer and 2-spacer showed higher ellipticities whereas 1-spacer and 3-spacer showed relatively lower ellipticities.

$V_DA_L$ peptides usually yielded M-type helical supramolecular aggregates except for 0-spacer compounds which showed P-type structure (**Figure 4, Table S3**). The intensity of the Cotton effects roughly followed an odd-even pattern indicating stark difference to the interaction in between π-π chromophores and the strength of subsequent exciton coupling. For example, the 2-spacer $V_DA_L$ molecule shows very weak Cotton effect and 0-spacer molecule did not show any bisignate Cotton effect, indicating that the PTP chromophores do not undergo exciton coupling as corroborated by UV-Vis signatures which did not show significant blue-shift under assembled conditions whereas 1- and 3-spacer molecules yielded very strong Cotton effects. We interpret the lack of a bisignate signal in the $V_DA_L$-0 and $V_LA_D$-0 assemblies to suggest that the PTP chromophores are in a chiral peptidic environment but are not interacting sufficiently strong to promote exciton coupling. Generally, larger magnitudes of Cotton effect indicate more organized

nanostructure formation but the possibility of the additive presence of both P-type and M-type nanostructure cannot be overruled.

$V_LA_D$ peptides also usually formed M-type helical supramolecular aggregates except for 3-spacer compounds which showed P-type structure (**Figure 4, Table S3**). Overall, odd-even effects were also apparent in the Cotton effect signatures among these peptides. 0-spacer and 2-spacer compounds did not show split Cotton band indicating absence of exciton coupling in between interacting chromophores whereas 1- and 3-spacer molecules showed Cotton effects. However, the magnitudes of the Cotton effects are relatively small across all the $V_LA_D$ peptides showing the subtle change in local environment in between interacting chromophores can have impact on the packing efficiency of the supramolecular nanostructures.

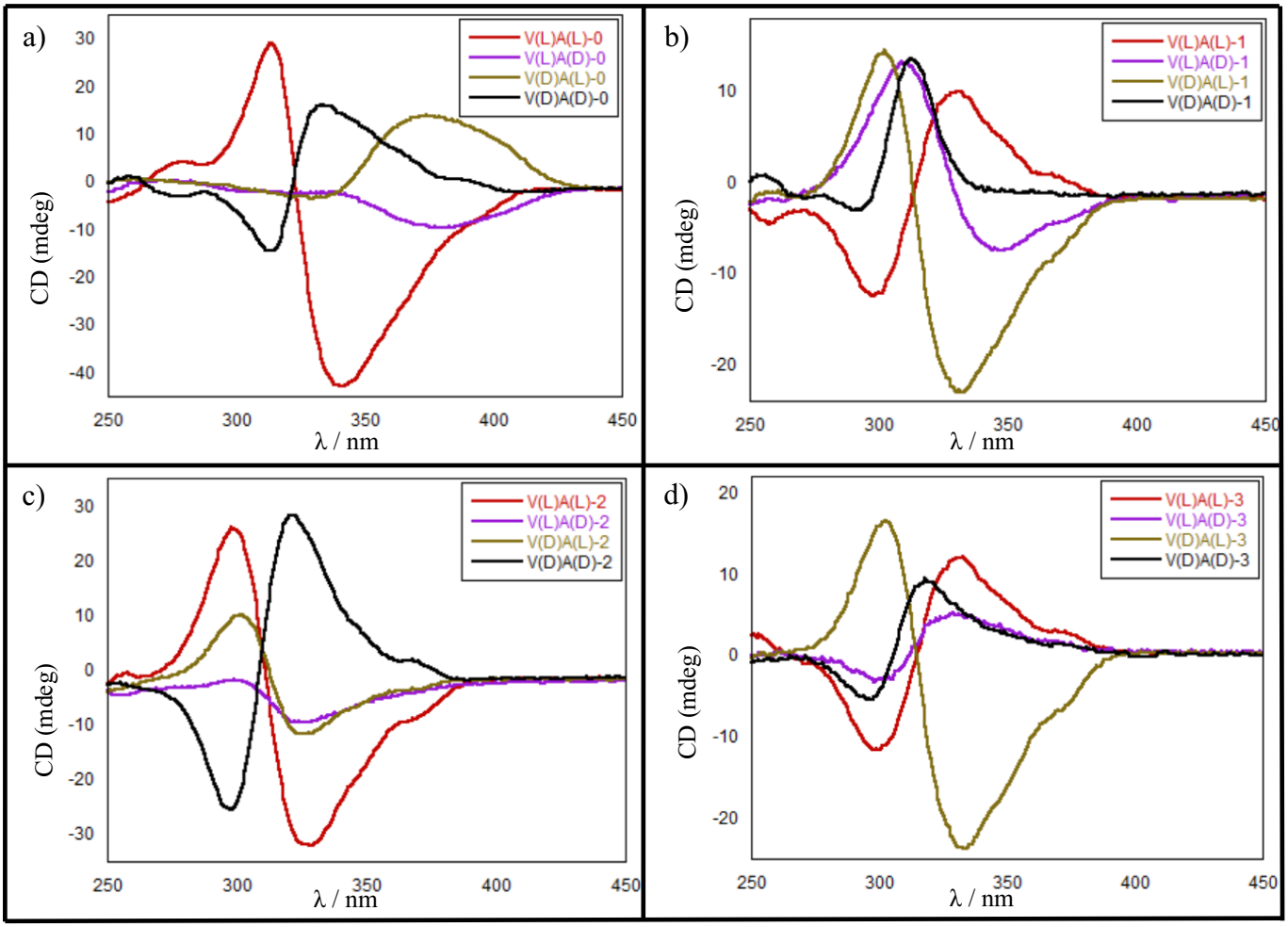


**Figure 4**. CD spectroscopy of (a) 0-spacer, (b) 1-spacer, (c) 2-spacer and (d) 3-spacer under acidic condition at a concentration of 25 μM. Basic solutions were made by adding 30 μL of KOH (2M) and acidified by adding 50 μL of HCl (2M) to the basic solution.

To further extend and test the influence of residue chirality upon supramolecular structure and properties, we prepared a peptide with a more remote D-stereogenic center ($V_DEV_LA_LG$-0) to compare with the all L-example. Our prior modeling and machine learning work identified this terminal valine not to play a significant role in the chiroptical induction within the nanostructures upon assembly.[63] This peptide yielded an absorption blue shift of ca. 28 nm upon going from unassembled to assembled solution in UV-Vis spectroscopy (**Figure 5a**) and showed featureless photoluminescence spectra (**Figure S59**) similar to $V_LA_L$-0. This indicates that the remote

stereogenic change presents no profound alteration on the assembly process. CD spectroscopy of $V_DEV_LA_LG$ also maintained a similar type of signature as of $V_LA_L$-0, only with lower intensity (**Figure 5b**), in contrast to the significant variation observed when key atoms/residues identified in our previous work were altered within the same series. Our findings suggest that switching the configuration of the constituent amino acids results in subtle variations of the intermolecular ordering and arrangement of the central chromophoric region after assembly, which affects the photophysical properties. These results suggest that 0-spacer and 2-spacer molecules (except $V_DA_L$) show similar characteristics of supramolecular chirality and 1-spacer and 3-spacer molecules (except $V_LA_D$) show similar characteristics.

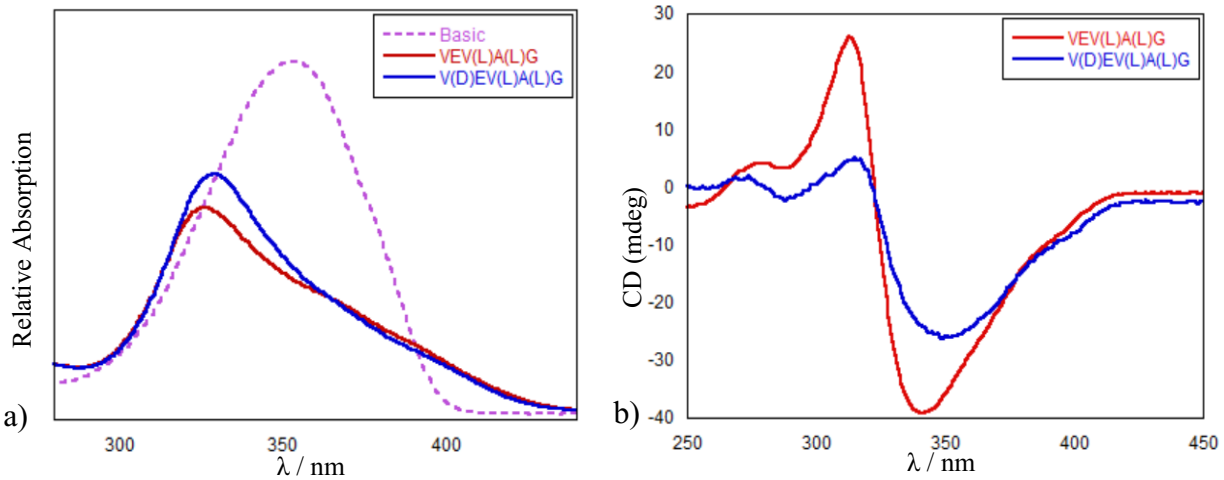


**Figure 5**. (a) UV-Vis spectroscopy and (b) CD spectroscopy of $V_LA_L$-0 and $V_DEV_LA_LG$-0 under acidic condition at a concentration of 25 μM. Basic solutions were made by adding 30 μL of KOH (2M) and acidified by adding 50 μL of HCl (2M) to the basic solution.

**Computational Studies.** As a point of comparison to the experimental studies we performed all-atom molecular dynamics simulations measuring the preferences in supramolecular chirality as a function of both spacer length and stereochemistry of the alanine and valine residues proximate to the π-conjugated core. Herein we adopt a previously employed method for measuring preferences

in supramolecular chirality[63] by probing the behavior of a dimerized pair of π-conjugated peptides. In taking this reductionist hypothesis, we assume that the supramolecular organization of the dimer pair, which can be comprehensively explored using enhanced sampling calculations, is representative of that within the full self-assembled aggregate. While this reductionist approach neglects higher-order multi-body effects that may influence supramolecular chirality, this minimal system is designed to preserve the salient physics while enabling comprehensive sampling of the thermally-accessible phase space and extraction of robust thermodynamic averages. Support for this reductionist viewpoint is provided in the broadly good agreement of the computational predictions with experimental observations in both the present work and our previous study[63]. The value of comprehensive sampling within a simple system is particularly illuminated in the relatively weak thermodynamic chiral preferences that may be very challenging to extract in larger, many-body systems that cannot be sampled exhaustively.

To accurately deduce supramolecular chirality preferences from simulation requires sampling the configurational phase space of a model system to evaluate whether M- or P-type conformations are thermodynamically preferred. While, in principle, unbiased simulations will eventually explore the relevant state space, in practice, they frequently fail to ergodically sample the state space due to large free-energy barriers making transitions between metastable states rare events that are inaccessible on the time scales of unbiased calculations. A number of enhanced sampling techniques are available to apply artificial biases and accelerate exploration in a pre-selected set of collective variables (CVs)[81-84]. In this work, we employ well-tempered metadynamics[72] as a popular and easy-to-use methodology that constructs a time-dependent bias potential to encourage sampling of unvisited regions of CV space and which we have previously applied to these π-conjugated peptide systems[63]. Once sampling is converged the simulation

samples freely and uniformly along the CVs and an estimate of the free energy landscape may be computed from the terminal bias potential that serves a "mold" of the underlying free energy surface[76, 85].

In brief, to accelerate sampling of configurations with varying supramolecular chirality we performed well-tempered metadynamics[72] along a single collective variable (CV) defined as the signed twist-angle $\theta$ between the dimer pair of $\pi$ -conjugated peptides (**Figure 6**). Defining $\boldsymbol{d}$ as the vector connecting the center of mass of, arbitrarily labeled, molecule 1 to molecule 2, and $\boldsymbol{m_1}$ and $\boldsymbol{m_2}$ as vectors between the terminal carbon atoms within the aromatic cores of molecule 1 and molecule 2, the twist angle is defined as:

$$\theta = arccos(\boldsymbol{m_1} \cdot \boldsymbol{m_2}) \cdot sgn((\boldsymbol{m_2} \times \boldsymbol{m_1}) \cdot \boldsymbol{d}) \qquad \textbf{Eqn. 1}$$

The first term in Eqn. 1 $arccos(\boldsymbol{m_1} \cdot \boldsymbol{m_2})$ computes the absolute angle between vectors $\boldsymbol{m_1}$ and $\boldsymbol{m_2}$ which is then endowed by a sign through the second term calculating the handedness through projection of the cross product $\boldsymbol{m_2} \times \boldsymbol{m_1}$ onto $\boldsymbol{d}$ and taking the sign. As defined, positive values of $\theta$ correspond to M-type (left-handed) stacks, whereas negative values of $\theta$ correspond to P-type (right-handed) stacking. Harmonic restraints in addition to the metadynamics bias are applied to ensure $\theta \in [-1.25, 1.25]$ and $|\boldsymbol{d}| < 0.6$ nm, which maintain integrity of the dimer and greatly accelerate sampling and convergence[63].

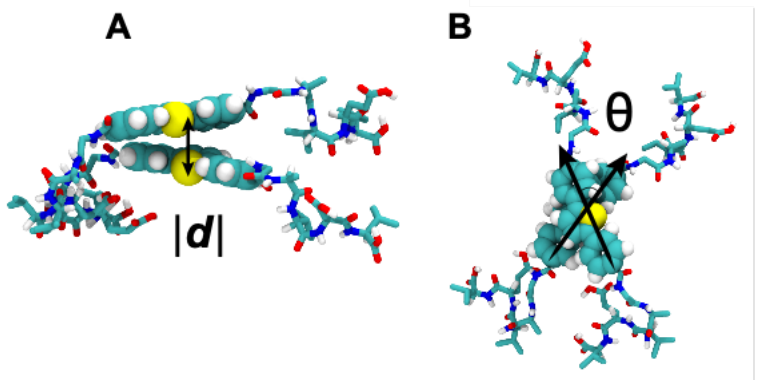


**Figure 6.** Schematic illustration of the metadynamics setup. (A) A single dimerized pair of π-conjugated peptides is prepared by initializing the COM separation |d| between the two peptides as |d| = 0.45 nm. A harmonic constraint is applied to control |d| < 0.6 nm to ensure the molecules remain dimerized throughout the simulation. (B) The signed twist angle $\theta$ between the two peptides (Eqn. 1) defines the collective variable along which sampling is enhanced by well-tempered metadynamics. Positive values of θ correspond to M-type (left-handed) stacks, whereas negative values of θ correspond to P-type (right-handed) stacking. A harmonic constraint is added to ensure $\theta \in$ [-1.25, 1.25] radians to avoid any unphysical "interlocked" conformations of the molecules while also helping to accelerate sampling and convergence. Molecules are visualized using VMD[86].

We evaluate preferences in supramolecular chirality by computing the relative probabilities of left- and right-handed dimer configurations. This analysis is in part motivated by the varying intensity of CD spectra observed in the different systems, suggesting that both M- and P-type stacks are present at different proportions depending on the relative intensities. Converged metadynamics comprehensively explores the CV coordinate throughout the simulation enabling efficient sampling of configurations with a diversity of twist angles $\theta$. $P(\theta)$ is then estimated by reweighting the biased distributions according to the externally applied potential[79]. Given the unbiased probability distribution $P(\theta)$ the probability of observing an M-type (left-handed, $\theta > 0$) stack is given by:

$$P(\theta > 0) = \frac{\int_0^{\frac{\pi}{2}} P(\theta) d\theta}{\int_{-\frac{\pi}{2}}^{\frac{\pi}{2}} P(\theta) d\theta} \quad \textbf{Eqn. 2}$$

Given $N$ system configurations recorded from a single well-tempered metadynamics simulation, an empirical estimate of the quantity $P(\theta > 0)$ may be calculated from the data as

$$P(\theta > 0) \approx \frac{\sum_{i=0}^{N} w_i \, |1.25> \theta_i > 0 \; and \; |d_i| < 0.6 \text{ nm}}{\sum_{i=0}^{N} w_i \, |1.25> \theta_i > -1.25 \; and \; |d_i| < 0.6 \text{ nm}} \quad \textbf{Eqn. 3}$$

where $w_i$ are the weights associated with configuration $i$ derived from all the applied biases and where we have restricted the summation to configurations $\theta_i \in [-1.25, 1.25]$ and $|d_i| < 0.6$ nm to reflect the conditions on the center of mass distance between the peptides for an associated dimer. (In the case of an unbiased simulation each weight would be $w_i = \frac{1}{N}$ and the procedure would effectively reduce to simply counting the number of configurations observed with left-handed chirality under the predefined restrictions. Unbiased calculations exhibit poor sampling of the complete range of $\theta$ and carry large statistical uncertainties, however, motivating the need for enhanced sampling calculations.) Standard errors in $P(\theta > 0)$ are estimated from the standard deviation taken over the five independent well-tempered metadynamics runs.

We present in **Figure 7** the calculated probabilities of observing M-type (left-handed) supramolecular chirality at all of the four spacer lengths and all four combinations of alanine and valine stereochemistries. These results are in good reasonable agreement with the experimental observations, with only $V_DA_L$-0 disagreeing outside of error bars. We observe these systems to exhibit relatively weak preferences for supramolecular chirality, as indicated by many of the probabilities lying near $P(\theta > 0) \approx 50\%$ and frequently spanning the 50% boundary within error bars. We find that only $V_DA_L$-0 and $V_LA_D$-2 present a definitive M-type preference, while all other

systems display only marginal stability where their preferences in supramolecular chirality can be interpreted, within error, as either M- or P-type. Unlike the odd-even effect spacer length has on supramolecular chirality within the $VEV_LA_LG$ family, neither simulation or experiment reports particularly strong trends correlating spacer length and amino acid stereochemistry to emergent preferences in supramolecular chirality. The broadly good agreement within error bars between experiment and computation provides support for the simulation approach as a viable means to perform virtual screening to predict supramolecular chiral preferences of candidate molecules at a higher-throughput and efficiency than would be possible by direct physical experimentation. We minimize statistical errors in our calculations by conducting comprehensive enhanced sampling of chirality of the dimer, but systematic errors associated with approximations in the force field and our adoption of a reductionist viewpoint focusing on a single isolated dimer pair[87]. It is conceivable that experimental agreement may be improved by incorporating higher-order multi-body effects in simulations comprising more molecules, but comprehensive sampling, identification of good collective variables for sampling, and extraction of the weak thermodynamic preferences in these large systems may prove challenging.

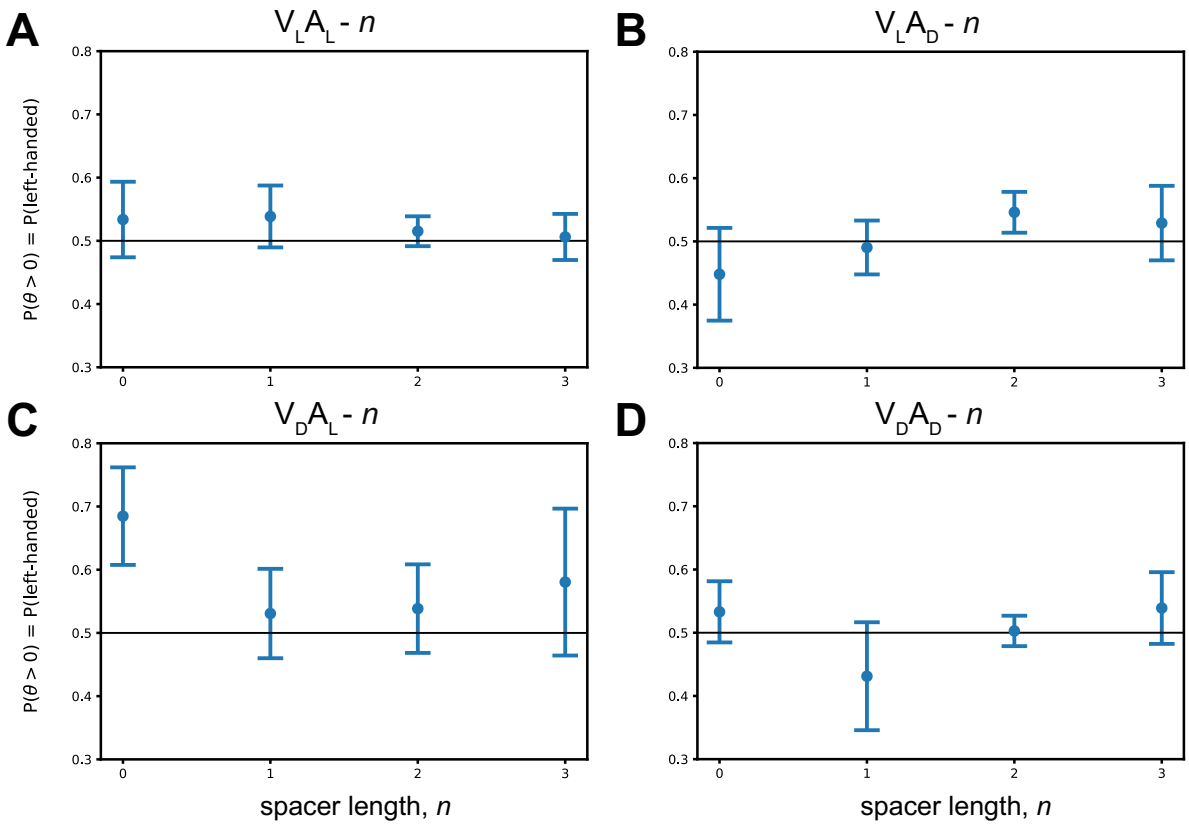


**Figure 7**. Probability of observing configurations with M-type (left-handed) supramolecular character as a function of spacer length *n* for each combination of valine and alanine stereochemistry (a) $V_LA_L$-*n*, (b) $V_LA_D$-*n*, (c) $V_DA_L$-*n*, and (d) $V_DA_D$-*n*. The probabilities P(θ>0) are calculated from well-tempered metadynamics simulation along the CV θ defined as the signed twist angle between a dimerized pair of pi-conjugated peptides according to the procedure outlined in Experimental Section. Error bars correspond to standard errors estimated from the standard deviation of calculated probabilities P(θ>0) over the five, converged, independent well-tempered metadynamics simulations conducted for each spacer length and stereochemistry.

## Conclusion:

We presented a detailed study on a series of peptide-spacer-π conjugates varying the configuration of constituent amino acids resulting in a broad range of absorption, emission, and chiroptical properties. Alteration of key atoms/residues previously identified by machine learning-aided analysis of all-atom molecular simulations modulated the experimentally-observed

supramolecular chirality of the assembled networks and the observed trends were largely corroborated by all-atom molecular modeling and enhanced sampling calculations. This study illuminates the value of designing molecules based on initial computational insight. UV-Vis, PL and CD spectroscopy showed that subtle differences in the molecular arrangement can significantly influence the arrangement of chromophores within the resulting nanostructures. Varied H-type aggregation was observed in UV-Vis spectra where a systematic progression of blue-shift was observed from modest change in molecular systems. Photoluminescence spectroscopy also showed a range of properties from vibronically structured to featureless emissions, indicating that varying degrees of exciton delocalization can be attained through simple changes in peptide primary structures. This is particularly important in the context of developing charge-transporting materials where the excitons can undergo a band-like or hopping transport. However, more important features were evident from CD spectra which showed how the change in spacer length dictated the formation of different superstructures even if the amino acid stereochemistry is changed. Prior computational work identified residues that were the key determinants of supramolecular chiral packing and motivated the present study[63]. Herein we show that computational predictions show broadly good agreement with experimental trends and offer a platform for virtual screening of candidate molecules to engineer desired supramolecular chirality. This systematic exploration of how the configuration of local amino acids impacts the electronic properties of hierarchical structures will be helpful to further explore bioelectronic properties of related supramolecular nanomaterials for potential energy-transporting applications.

**Notes:** A.L.F. is a consultant of Evozyne and a co-author of US Provisional Patents 62/853,919 and 62/900,420.

**Acknowledgement:** This research is based upon work supported by the National Science Foundation's Designing Materials to Revolutionize and Engineer our Future (DMREF) program (Grant Nos. DMR-1728947 and DMR-1841807). K.S. is supported by the National Science Foundation's Graduate Research Fellowship (Grant No. DGE-1746045). We also acknowledge support from Johns Hopkins University. We thank the Center for Molecular Biophysics (JHU) for the use of a circular dichroism spectrometer, and Prof. Hai-Quan Mao for the use of a Zetasizer for the dynamic light scattering experiments. This work was completed in part with resources provided by the University of Chicago Research Computing Center. We gratefully acknowledge computing time on the University of Chicago high-performance GPU-based cyberinfrastructure (Grant No. DMR-1828629).

**Supporting Information.** Synthesis procedures, ESI mass spectrometry spectra, HPLC data, NMR spectra, TEM images, DLS data, FT-IR spectra, UV-vis spectra, PL spectra, CD spectra, and metadynamics convergence.

**References:**

1. Liu, M.; Zhang, L.; Wang, T. Supramolecular Chirality in Self-Assembled Systems. *Chem. Rev*. **2015**, *115*, 7304−7397.
2. Yashima, E.; Ousaka, N.; Taura, D.; Shimomura, K.; Ikai, T.; Maeda, K. Supramolecular Helical Systems: Helical Assemblies of Small Molecules, Foldamers, and Polymers with Chiral Amplification and Their Functions. *Chem. Rev*. **2016**, *116*, 13752−13990.
3. Yashima, E.; Maeda, K.; Iida, H.; Furusho, Y.; Nagai, K. Helical Polymers: Synthesis, Structures, and Functions. *Chem. Rev*. **2009**, *109* (11), 6102–6211.
4. Xing, P.; Zhao, Y. Controlling Supramolecular Chirality in Multicomponent Self-Assembled Systems. *Acc. Chem. Res.* **2018**, *51* (9), 2324–2334.
5. Edwards, W.; Smith, D. K. Enantioselective Component Selection in Multicomponent Supramolecular Gels. *J. Am. Chem. Soc*. **2014**, *136*, 1116-1124.
6. Patterson, D.; Schnell, M.; Doyle, J. M. Enantiomer-Specific Detection of Chiral Molecules via Microwave Spectroscopy. *Nature* **2013**, *497*, 475−477.
7. Jiang, J.; Meng, Y.; Zhang, L.; Liu, M. Self-Assembled Single-Walled Metal-Helical Nanotube (M-HN): Creation of Efficient Supramolecular Catalysts for Asymmetric Reaction. *J. Am. Chem. Soc.* **2016**, *138* (48), 15629-15635.

8. Kumar, M.; Brocorens, P.; Tonnele, C.; Beljonne, D.; Surin, M.; George, S. J. A dynamic supramolecular polymer with stimuli-responsive handedness for in situ probing of enzymatic ATP hydrolysis. *Nat. Commun.* **2014**, *5*, 5793.
9. Liu, G.-F.; Zhang, D.; Feng, C.-L. Control of ThreeDimensional Cell Adhesion by the Chirality of Nanofibers in Hydrogels. *Angew. Chem., Int. Ed*. **2014**, *53*, 7789−7793.
10. Lee, C. C.; Grenier, C.; Meijer, E. W.; Schenning, A. P. H. J. Preparation and characterization of helical self-assembled nanofibers. *Chem. Soc. Rev*. **2009**, *38*, 671−683.
11. Tovar, J. D. Supramolecular Construction of Optoelectronic Biomaterials. *Acc. Chem. Res.* **2013**, *46* (7), 1527–1537.
12. Raymond, D. M.; Nilsson, B. L. Multicomponent Peptide Assemblies. *Chem. Soc. Rev*. **2018**, *47*, 3659−3720.
13. Gazit, E. Self-Assembled Peptide Nanostructures: The Design of Molecular Building Blocks and Their Technological Utilization. *Chem. Soc. Rev*. **2007**, *36*, 1263−1269.
14. Ulijn, R. V.; Smith, A. M. Designing peptide based nanomaterials. *Chem. Soc. Rev*. **2008**, *37*, 664−675.
15. Ajayaghosh, A.; George, S. J.; Schenning, A. P. H. J. HydrogenBonded Assemblies of Dyes and Extended π-Conjugated Systems. In Würthner, F., Eds.; *Supermolecular Dye Chemistry*; Topics in Current Chemistry; Springer: Berlin, 2005: Vol. 258, pp 83−118.
16. Li, Y.; Li, B.; Fu, Y.; Lin, S.; Yang, Y. Solvent-Induced Handedness Inversion of Dipeptide Sodium Salts Derived from Alanine. *Langmuir* **2013**, *29*, 9721−9726.
17. Xue, S.; Xing, P.; Zhang, J.; Zeng, Y.; Zhao, Y. Diverse Role of Solvents in Controlling Supramolecular Chirality. *Chem. Eur. J*. **2019**, *25*, 7426 – 7437.
18. Huang, Y.; Hu, J.; Kuang, W.; Wei, Z.; Faul, C. F. J. Modulating Helicity through Amphiphilicity — Tuning Supramolecular Interactions for the Controlled Assembly of Perylenes. *Chem. Comm.* **2011**, 47, 5554–5556.
19. Kulkarni, C.; Korevaar, P. A.; Bejagam, K. K.; Palmans, A. R. A.; Meijer, E. W.; George, S. J. Solvent Clathrate Driven Dynamic Stereomutation of a Supramolecular Polymer with Molecular Pockets. *J. Am. Chem. Soc*. **2017**, *139*, 13867−13875.
20. Hamley, I. W.; Dehsorkhi, A.; Castelletto, V.; Furzeland, S.; Atkins, D.; Seitsonen, J.; Ruokolainen, J. Reversible Helical Unwinding Transition of a Self-Assembling Peptide Amphiphile. *Soft Matter* **2013**, *9*, 9290−9293.
21. Peterca, M.; Imam, M. R.; Ahn, C. H.; Balagurusamy, V. S.; Wilson, D. A.; Rosen, B. M.; Percec, V. Transfer, Amplification, and Inversion of Helical Chirality Mediated by Concerted Interactions of C3-Supramolecular Dendrimers. *J. Am. Chem. Soc*. **2011**, *133*, 2311−2328.
22. Kim, Y.; Li, H.; He, Y.; Chen, X.; Ma, X.; Lee, M. Collective helicity switching of a DNA–coat assembly. *Nat. Nanotechnol*. **2017**, *12*, 551-556.
23. Kurouski, D.; Lombardi, R. A.; Dukor, R. K.; Lednev, I. K.; Nafie, L. A. Direct Observation and pH Control of Reversed Supramolecular Chirality in Insulin Fibrils by Vibrational Circular Dichroism. *Chem. Commun*. **2010**, *46*, 7154−7156.
24. Yagai, S.; Yamauchi, M.; Kobayashi, A.; Karatsu, T.; Kitamura, A.; Ohba, T.; Kikkawa, Y. Control Over Hierarchy Levels in the Self-Assembly of Stackable Nanotoroids. *J. Am. Chem. Soc*. **2012**, 134, 18205−18208.

25. Kumar, J.; Nakashima, T.; Kawai, T. Inversion of Supramolecular Chirality in Bichromophoric Perylene Bisimides: Influence of Temperature and Ultrasound. *Langmuir* **2014**, *30*, 6030−6037.
26. Ogoshi, T.; Akutsu, T.; Yamafuji, D.; Aoki, T.; Yamagishi, T. A. Solvent- and Achiral-Guest-Triggered Chiral Inversion in a Planar Chiral Pseudo[1]catenane. *Angew. Chem., Int. Ed*. **2013**, *52*, 8111−8115.
27. Liu, G. F.; Zhu, L. Y.; Ji, W.; Feng, C. L.; Wei, Z. X. Inversion of the Supramolecular Chirality of Nanofibrous Structures through Co-Assembly with Achiral Molecules. *Angew. Chem., Int. Ed*. **2016**, *55*, 2411−2415.
28. Wang, M.; Zhou, P.; Wang, J.; Zhao, Y.; Ma, H.; Lu, J. R.; Xu, H. Left or Right: How Does Amino Acid Chirality Effect the Handedness of Nanostructures Self-Assembled from Short Amphiphilic Peptides? *J. Am. Chem. Soc*. **2017**, *139*, 4185-4194.
29. Marchesan, S.; Easton, C. D.; Styan, K. E.; Waddington, L. J.; Kushkaki, F.; Goodall, L.; McLean, K. M.; Forsythe, J. S.; Hartley, P. G. Chirality Effects at each Amino Acid Position on Tripeptide Self-assembly into Hydrogel Biomaterials. *Nanoscale* **2014**, *6*, 5172−5180.
30. Cui, H.; Cheetham, A. G.; Pashuck, E. T.; Stupp, S. I. Amino Acid Sequence in Constitutionally Isomeric Tetrapeptide Amphiphiles Dictates Architecture of One-Dimensional Nanostructures. *J. Am. Chem. Soc*. **2014**, *136*, 12461−12468.
31. Xing, Q.; Zhang, J.; Xie, Y.; Wang, Y.; Qi, W.; Rao, H.; Su, R.; He, Z. Aromatic Motifs Dictate Nanohelix Handedness of Tripeptides. *ACS Nano* **2018**, *12*, 12305−12314.
32. Lin, S.; Li, Y.; Li, B.; Yang, Y. Control of the Handedness of Self-Assemblies of Dipeptides by the Chirality of Phenylalanine and Steric Hindrance of Phenylglycine. *Langmuir* **2016**, *32*, 7420− 7426.
33. Shi, J.; Du, X.; Yuan, D.; Zhou, J.; Zhou, N.; Huang, Y.; Xu, B. D-Amino Acid Modulate the Cellular Response of Enzymatic-Instructed Supramolecular Nanofibers of Small Peptides. *Biomacromolecules* **2014**, *15*, 3559−3568.
34. Fu, Y.; Li, B.; Huang, Z.; Li, Y.; Yang, Y. Terminal is Important for the Helicity of the Self-Assemblies of Dipeptides Derived from Alanine. *Langmuir* **2013**, *29*, 6013−6017.
35. Panda, S. S.; Katz, H. E.; Tovar, J. D. Solid-State Electrical Applications of Protein and Peptide Based Nanomaterials. *Chem. Soc. Rev*. **2018**, *47*, 3640−3658.
36. Draper, E. R.; Walsh, J. J.; McDonald, T. O.; Zwijnenburg, M. A.; Cameron, P. J.; Cowan, A. J.; Adams, D. J. Air-stable Photoconductive Films Formed from Perylene Bisimide Gelators. *J. Mater. Chem. C* **2014**, *2*, 5570−5575.
37. Nalluri, S. K. M.; Berdugo, C.; Javid, N.; Frederix, P. W. J. M.; Ulijn, R. V. Biocatalytic Self-Assembly of Supramolecular Charge Transfer Nanostructures Based on n-type Semiconductor-Appended Peptides. *Angew. Chem., Int. Ed*. **2014**, *53*, 5882−5887.
38. Khalily, M. A.; Bakan, G.; Kucukoz, B.; Topal, A. E.; Karatay, A.; Yaglioglu, H. G.; Dana, A.; Guler, M. O. Fabrication of Supramolecular n/p-Nanowires via Coassembly of Oppositely Charged Peptide-Chromophore Systems in Aqueous Media. *ACS Nano* **2017**, *11*, 6881−6892.
39. Tsai, W. W.; Tevis, I. D.; Tayi, A. S.; Cui, H.; Stupp, S. I. Semiconducting Nanowires from Hairpin-Shaped Self-Assembling Sexithiophenes. *J. Phys. Chem. B* **2010**, *114*, 14778−14786.

40. Besar, K.; Ardona, H. A. M.; Tovar, J. D.; Katz, H. E. Demonstration of Hole Transport and Voltage Equilibriation in Self-Assembled π-Conjugated Peptide Nanostructures Using Field-Effect Transistor Architectures. *ACS Nano* **2015**, *9*, 12401−12409.
41. Eakins, G. L.; Pandey, R.; Wojciechowski, J. P.; Zheng, H. Y.; Webb, J. E. A.; Valery, C.; Thordarson, P.; Plank, N. O. V; Gerrard, J.́ A.; Hodgkiss, J. M. Functional Organic Semiconductors Assembled via Natural Aggregating Peptides. *Adv. Funct. Mater*. **2015**, *25*, 5640− 5649.
42. Shao, H.; Seifert, J.; Romano, N. C.; Gao, M.; Helmus, J. J.; Jaroniec, C. P.; Modarelli, D. A.; Parquette, J. R. Amphiphilic SelfAssembly of an n-Type Nanotube. *Angew. Chem., Int. Ed*. **2010**, *49*, 7688−7691.
43. Channon, K. J.; Devlin, G. L.; MacPhee, C. E. Efficient Energy Transfer within Self-Assembling Peptide Fibers: A Route to Light-Harvesting Nanomaterials. *J. Am. Chem. Soc*. **2009**, *131*, 12520–12521.
44. Stone, D. A.; Hsu, L.; Stupp, S. I. Self-Assembling Quinquethiophene−oligopeptide Hydrogelators. *Soft Matter* **2009**, *5*, 1990−1993.
45. Wall, B. D.; Diegelmann, S. R.; Zhang, S.; Dawidczyk, T. J.; Wilson, W. L.; Katz, H. E.; Mao, H. Q.; Tovar, J. D. Aligned Macroscopic Domains of Optoelectronic Nanostructures Prepared via Shear-Flow Assembly of Peptide Hydrogels. *Adv. Mater*. **2011**, *23*, 5009−5014.
46. Sanders, A. M.; Dawidczyk, T. J.; Katz, H. E.; Tovar, J. D. Peptide-Based Supramolecular Semiconductor Nanomaterials via Pd-Catalyzed Solid-Phase "Dimerizations. *ACS Macro Lett*. **2012**, *1*, 1326−1329.
47. Amit, M.; Yuran, S.; Gazit, E.; Reches, M.; Ashkenasy, N. Tailor-Made Functional Peptide Self-Assembling Nanostructures. *Adv. Mater*. **2018**, *30*, 1707083.
48. Lee, T.; Panda, S. S.; Tovar, J. D.; Katz, H. E. Unusually Conductive Organic–Inorganic Hybrid Nanostructures Derived from Bio-Inspired Mineralization of Peptide/Pi-Electron Assemblies. *ACS Nano* **2020**, 10.1021/acsnano.9b07911.
49. Draper, E. R.; Archibald, L. J.; Nolan, M. C.; Schweins, R.; Zwijnenburg, M. A.; Sproules, S.; Adams, D. J. Controlling Photoconductivity in PBI Films by Supramolecular Assembly. *Chem. - Eur. J*. **2018**, *24*, 4006−4010.
50. Schillinger, E. K.; Mena-Osteritz, E.; Hentschel, J.; Börner, H. G.; Bauerle, P. Oligothiophene versus¨β-Sheet Peptide: Synthesis and Self-Assembly of an Organic Semiconductor-Peptide Hybrid. *Adv. Mater*. **2009**, *21*, 1562−1567.
51. Nelli, S. R.; Lin, J.-H.; Nguyen, T. N. A.; Tseng, D. T-H.; Talloj, S. K.; Lin, H.-C. Influence of amino acid side chains on the formation of two component self-assembling nanofibrous hydrogels. *New J. Chem*. **2017**, *41*, 1229−1234.
52. Mba, M.; Moretto, A.; Armelao, L.; Crisma, M.; Toniolo, C.; Maggini, M. Synthesis and Self-Assembly of Oligo(p-phenylenevinylene) Peptide Conjugates in Water. *Chem. - Eur. J*. **2011**, *17*, 2044− 2047.
53. Kumar, M.; Ing, N. L.; Narang, V.; Wijerathne, N.; Hochbaum, A. I.; Ulijn, R. V. Amino Acid-Encoded Biocatalytic Self-Assembly Enables the Formation of Transient Conducting Nanostructures. *Nat. Chem*. **2018**, *10*, 696−703.

54. Kumar, R. J.; MacDonald, J. M.; Singh, T. B.; Waddington, L. J.; Holmes, A. B. Hierarchical Self-Assembly of Semiconductor Functionalized Peptide α-Helices and Optoelectronic Properties. *J. Am. Chem. Soc*., **2011**, *133*, 8564–8573
55. Pandeeswar, M.; Avinash, M. B.; Govindaraju, T. Chiral Transcription and Retentive Helical Memory: Probing Peptide Auxiliaries Appended with Naphthalenediimides for Their One-Dimensional Molecular Organization. *Chem. Eur. J.* **2012**, *18*, 4818−4822.
56. Marty, R.; Nigon, R.; Leite, D.; Frauenrath, H. Two-Fold Odd-Even Effect in Self-Assembled Nanowires from Oligopeptide Polymer-Substituted Perylene Bisimides. *J. Am. Chem. Soc*. **2014**, *136*, 3919−3927.
57. Schillinger, E. K.; Kümin, M.; Digennaro, A.; Mena-Osteritz, E.; Schmid, S.; Wennemers, H.; Bauerle, P. Guiding Suprastructure Chirality of an Oligothiophene by a Single Amino Acid. *Chem. Mater*. **2013**, *25*, 4511−4521.
58. Selegård, R.; Rouhbakhsh, Z.; Shirani, H.; Johansson, L. B. G.; Norman, P.; Linares, M.; Aili, D.; Nilsson, K. P. R. Distinct Electrostatic Interactions Govern the Chiro-Optical Properties and Architectural Arrangement of Peptide−Oligothiophene Hybrid Materials. *Macromolecules* **2017**, *50*, 7102−7110.
59. Lopez-Andarias, A.; Lo´pez-Andarias, J.; Atienza, C.; Chicho´ n,´ F. J.; Carrascosa, J. L.; Martín, N. Tuning Optoelectronic and Chiroptic Properties of Peptide-Based Materials by Controlling the Pathway Complexity. *Chem. - Eur. J*. **2018**, *24*, 7755−7760.
60. Garifullin, R.; Guler, M. O. Supramolecular Chirality in Self-Assembled Peptide Amphiphile Nanostructures. *Chem. Commun*. **2015**, *51*, 12470−12473.
61. Wang, Y.; Qi, W.; Huang, R.; Yang, X.; Wang, M.; Su, R.; He, Z. Rational Design of Chiral Nanostructures from Self-Assembly of a Ferrocene-Modified Dipeptide. *J. Am. Chem. Soc*. **2015**, *137*, 7869−7880.
62. Kang, M.; Zhang, P.; Cui, H.; Loverde, S. M. π-π Stacking Mediated Chirality in Functional Supramolecular Filaments. *Macromolecules* **2016**, *49*, 994−1001.
63. Panda, S. S.; Shmilovich, K.; Ferguson, A. L.; Tovar, J. D. Controlling Supramolecular Chirality in Peptide-π-Peptide Networks by Variation of the Alkyl Spacer Length. *Langmuir* **2019**, *35*, 14060−14073.
64. Abraham, M. J.; Murtola, T.; Schulz, R.; Smith, J. C.; Hess, B.; Lindahl, E. GROMACS: High Performance Molecular Simulations through Multi-Level Parallelism from Laptops to Supercomputers. *SoftwareX* **2015**, 1-2, 19−25.
65. Tribello, G. A.; Bonomi, M.; Branduardi, D.; Camilloni, C.; Bussi, G. PLUMED 2: New Feathers for an Old Bird. *Comput. Phys. Commun*. **2014**, 185 (2), 604−613.
66. Koziara, K. B.; Stroet, M.; Malde, A. K.; Mark, A. E. Testing and Validation of the Automated Topology Builder (ATB) Version 2.0: Prediction of Hydration Free Enthalpies. *J. Comput.-Aided Mol. Des*. **2014**, 28, 221−233.
67. Schmid, N.; Eichenberger, A. P.; Choutko, A.; Riniker, S.; Winger, M.; Mark, A. E.; van Gunsteren, W. F. Definition and Testing of the GROMOS Force-Field Versions 54A7 and 54B7. *Eur. Biophys. J*. **2011**, 40, 843−856.
68. Berendsen, H. J. C.; Postma, J. P. M.; Gunsteren, W. F. Van; Hermans, J. Interaction Models for Water in Relation to Protein Hydration. Pullman, B., Ed.; In *Intermolecular Forces. The*

*Jerusalem Symposia on Quantum Chemistry and Biochemistry; Springer: Dordrecht, 1981*: pp 331−342.
69. Hockney, R. W. *Computer Simulation Using Particles*; CRC Press: Boca Raton, 1988.
70. Hess, B.; Bekker, H.; Berendsen, H. J. C.; Fraaije, J. G. E. M. LINCS: A Linear Constraint Solver for Molecular Simulations. *J. Comput. Chem*. **1997**, 18 (12), 1463−1472.
71. Essmann, U.; Perera, L.; Berkowitz, M. L. A smooth particle mesh Ewald method. *J. Chem. Phys.* **1995**, 103 (19), 8577−8593.
72. Barducci, A.; Bussi, G.; Parrinello, M. Well-Tempered Metadynamics: A Smoothly Converging and Tunable Free-Energy Method. *Phys. Rev. Lett*. **2008**, 100, 020603.
73. Bussi, G.; Donadio, D.; Parrinello, M. Canonical sampling through velocity rescaling. *J. Chem. Phys*. **2007**, 126, 014101.
74. Parrinello, M.; Rahman, A. Polymorphic transitions in single crystals: A new molecular dynamics method. *J. Appl. Phys*. **1981**, 52 (12), 7182−7190.
75. Frenkel, D.; Smit, B. *Understanding Molecular Simulation: From Algorithms to Applications*; Academic Press: London, 2001.
76. Laio, A.; Gervasio, F. L. Metadynamics: a method to simulate rare events and reconstruct the free energy in biophysics, chemistry and material science. *Rep. Prog. Phys.* **2008**, *71*, 126601.
77. Wall, B. D.; Zacca, A. E.; Sanders, A. M.; Wilson, W. L.; Ferguson, A. L.; Tovar, J. D. Supramolecular Polymorphism: Tunable Electronic Interactions within π-Conjugated Peptide Nanostructures Dictated by Primary Amino Acid Sequence. *Langmuir* **2014**, *30*, 5946−5956.
78. Kasha, M.; Rawls, H. R.; El-Bayoumi, M. A. The Exciton Model in Molecular Spectroscopy. *Pure Appl. Chem*. **1965**, *11*, 371−392.
79. Kelly, S. M.; Price, N. C. The Use of Circular Dichroism in the Investigation of Protein Structure and Function. *Curr. Protein Pept. Sci*. **2000**, *1*, 349−384.
80. Harada, N.; Nakanishi, K. *Circular Dichroic Spectroscopy - Exciton Coupling in Organic Stereochemistry*; University Science Books: Mill Valley, CA, 1983.
81. Patey, G. N.; Valleau, J. P. A Monte Carlo method for obtaining the interionic potential of mean force in ionic solution. *J. Chem. Phys*. **1975**, *63*, 2334-2339
82. Carter, E. A.; Ciccotti, G.; Hynes, J. T.; Kapral, R. Constrained reaction coordinate dynamics for the simulation of rare events. *Chem. Phys. Lett*. **1989**, *5*, 472-477.
83. Darve, E. Calculating free energies using average force. *J. Chem. Phys*. **2001**, *115*, 9169-9183.
84. Laio, A.; Parrinello, M. Escaping free-energy minima. *Proc. Natl. Acad. Sci. U. S. A*. **2002**, *99*, 12562-12566.
85. Bussi, G.; Laio, A. Using metadynamics to explore complex free-energy landscapes. *Nat. Rev. Phys*. **2020**, *2*, 200-212.
86. Humphrey, W.; Dalke, A.; Schulten, K. VMD: Visual Molecular Dynamics. *J. Mol. Graphics* **1996**, *14*, 33−38.
87. Karplus, M.; Petsko, G. A. Molecular dynamics simulations in biology. *Nature*, **1990**, *347*, 631-639.

**Table of Content Figure**